SCIENTIFIC Publishing Limited

New Energy Exploitation and Application

http://ojs.ukscip.com/journals/neea

Article

Thermal Conductivity of $CaSrFe_{0.75}Co_{0.75}Mn_{0.5}O_{6-\delta}$

Gillian Medicine Cloud, Mandy Guinn and Ram Krishna Hona *

Environmental Science Department, United Tribes Technical College, Bismarck, ND 58504, USA
* Correspondence: rhona@uttc.edu; Tel.: (701) 221-1329

Received: 2 February 2024; **Revised**: 1 March 2024; **Accepted**: 7 March 2024; **Published**: 14 March 2024

Abstract: $CaSrFe_{0.75}Co_{0.75}Mn_{0.5}O_{6-\delta}$, an oxygen-deficient perovskite, had been reported for its better electrocatalytic properties of oxygen evolution reaction. It is essential to investigate different properties such as the thermal conductivity of such efficient functional materials. The thermal conductivity of $CaSrFe_{0.75}Co_{0.75}Mn_{0.5}O_{6-\delta}$ is a critical parameter for understanding its thermal transport properties and potential applications in energy conversion and electronic devices. In this study, the authors present an investigation of the thermal conductivity of $CaSrFe_{0.75}Co_{0.75}Mn_{0.5}O_{6-\delta}$ at room temperature for its thermal insulation property study. Experimental measurement was conducted using a state-of-the-art thermal characterization technique, Thermtest thermal conductivity meter. The thermal conductivity of $CaSrFe_{0.75}Co_{0.75}Mn_{0.5}O_{6-\delta}$ was found to be 0.724 W/m/K at 25 °C, exhibiting a notable thermal insulation property i.e., low thermal conductivity.

Keywords: XRD; solid-state reaction; thermal conductivity; perovskite oxides

1. Introduction

Perovskite oxides exhibit a diverse array of intriguing properties, including ferroelectricity [1], piezoelectricity [2], superconductivity [3], and catalytic activity [4–6], making them highly valuable in applications across electronics, catalysis, and energy storage. Recent research has focused on the potential technological applications of perovskite oxides, spanning solid oxide fuel cells [7], metal-air batteries [8], lithium batteries [9], electrocatalysis [10], thermal insulation [11], sensors [12,13], and photovoltaics [14]. The role of oxygen is crucial for these materials to manifest functional properties, particularly in transition-metal oxides, showcasing excellent catalytic behavior [15]. Perovskite-type systems, with the general formula ABO_3, where A is typically an alkaline-earth metal or lanthanide, and B is usually a transition metal, present significant interest. Oxygen-deficient perovskite materials, such as $CaSrFe_{1-x}Co_{1-x}Mn_{2x}O_{6-\delta}$, with vacancy-disordered systems, have gained attention for their unique properties [10]. Notably, the composition with x = 0.25 in the series $CaSrFe_{1-x}Co_{1-x}Mn_{2x}O_{6-\delta}$ gives a formula of $CaSrFe_{0.75}Co_{0.75}Mn_{0.5}O_{6-\delta}$ which demonstrated remarkable catalytic efficiency in oxygen and green hydrogen generation.

Since $CaSrFe_{0.75}Co_{0.75}Mn_{0.5}O_{6-\delta}$ outperformed the electrocatalytic behavior of water splitting for oxygen and hydrogen production, we are interested in studying its thermal insulation nature. $CaSrFe_{0.75}Co_{0.75}Mn_{0.5}O_{6-\delta}$ has been reported for its structural analysis by powder XRD and neutron diffraction [16]. However, its thermal insulation nature has not been reported yet. We explore the thermal properties of $CaSrFe_{0.75}Co_{0.75}Mn_{0.5}O_{6-\delta}$ that may contribute not only to the advancement of material science but also open avenues for the development of innovative technologies that rely on superior thermal insulation characteristics.

https://doi.org/10.54963/neea.v3i1.222

2. Experimental

The synthesis of $CaSrFe_{0.75}Co_{0.75}Mn_{0.5}O_{6-\delta}$ involved the solid-state reaction method conducted at elevated temperatures. Precursor compounds are the carbonates and oxides such as $CaCO_3$, $SrCO_3$, Fe_2O_3, Co_3O_4, and Mn_2O_3. Precise weighing and homogenous mixing of these individual powders in stoichiometric proportions were carried out using an agate mortar and pestle. Subsequently, pellets were methodically prepared from the powder blend under a pressure of 19 Mpa or a force of 3 tons, followed by calcination at 1000 °C for 24 hours. The resulting pellets underwent cooling to room temperature, regrinding, and repalletization. The sintering process occurred at 1200 °C for 24 hours, maintaining a constant heating rate of 100 °C/h throughout both the calcination and sintering processes.

To evaluate the crystal structure and phase purity of the synthesized material, powder X-ray diffraction (PXRD) utilizing Cu Kα1 and Kα2 radiations was employed. Rietveld refinements of the XRD data were conducted using the GSAS software and the EXPEGUI interface. Additionally, microstructural studies were performed by scanning micrographs of the materials through Thermo Fisher Apreo C LoVac Field Emission Scanning Electron Microscope. Widely applied iodometric titrations were carried out to determine the degree of oxygen deficiency in $CaSrFe_{0.75}Co_{0.75}Mn_{0.5}O_{6-\delta}$ [10,17,18]. Iodometric titrations were performed by dissolving about 50 mg of the sample and excess KI (~2 g) in 100 mL of 1 M HCl. A total of 5 mL of the solution was then pipetted out, and the iodine that had been generated in the solution was titrated using 0.025 M $Na_2S_2O_3$. Near the end point of the titration, 10 drops of a starch solution were added to act as an indicator. All steps were carried out under an argon atmosphere.

The thermal conductivities of the materials were investigated using a Thermtest thermal conductivity meter, MP-2 with TPS-4. This method is based on the principle of the Transient Plane Source Method. A circular disc with a diameter of 13 mm/25 mm and a thickness of 3 mm was placed on the flat sensor of the Thermtest device, and the thermal conductivity was measured at room temperature.

3. Results and Discussion

3.1. Structure

$CaSrFe_{0.75}Co_{0.75}Mn_{0.5}O_{6-\delta}$ is classified as an oxygen-deficient cubic perovskite oxide, possessing the Pm-3m space group. Figure 1 illustrates its X-ray diffraction (XRD) data, while Table 1 provides the Rietveld refined cell parameters. The obtained results align with those reported previously, reinforcing the consistency of our findings with existing literature. As highlighted in the introduction, oxygen-deficient perovskites adhere to a general formula represented as ABO3-δ or $A_2B_2O_{6-\delta}$, where A represents an alkaline earth metal and B denotes a 3d or 4d transition metal. In the case of $CaSrFe_{0.75}Co_{0.75}Mn_{0.5}O_{6-\delta}$, the A-site is occupied by Ca and Sr, while the B-site is occupied by Fe, Co, and Mn.

Upon close examination of Figure 2, it becomes apparent that the Fe/Co/Mn atoms, represented by green spheres, are encompassed by six oxygen atoms (small red spheres) occupying octahedral positions. To elucidate the octahedral structures, imaginary planes (depicted as black planes) connecting oxygen atoms are drawn. This arrangement forms BO_6 octahedra, highlighting that Fe/Co/Mn atoms exhibit a consistent coordination number of 6 throughout the crystal lattice, as depicted in Figure 2a, excluding the positions with oxygen deficiency (not shown due to uncertainty).

Given the composition $CaSrFe_{0.75}Co_{0.75}Mn_{0.5}O_{6-\delta}$, it signifies that Fe and Co collectively occupy 75% of the B-site positions, with each element individually taking up 37.5% of the total B-site positions. Meanwhile, Mn occupies 25% of the B-site positions. As illustrated in Figure 2b, the largest sphere in whitish grey, representing Ca/Sr atoms, is surrounded by eight octahedra. Ca and Sr share A-site positions equally, each occupying 50% of the A-sites. Ca/Sr atoms display a 12-coordinated arrangement, except in positions with oxygen deficiency (not shown due to uncertainty).

The octahedra connect to each other through corner sharing via oxygen, forming a bonding pattern denoted as B-O-B, where B represents Fe/Co/Mn. The B-O-B bond angle is consistently 180°. Figure 3 shows the SEM image of $CaSrFe_{0.75}Co_{0.75}Mn_{0.5}O_{6-\delta}$. The material is observed porous with diffused grains and without clear grain

boundary. The iodometric titrations showed $\delta \approx 0.56$ for this compound, which indicates a significant degree of oxygen deficiency.

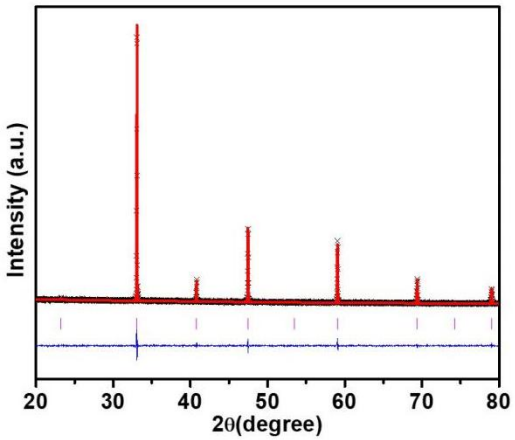

Figure 1. Rietveld refinement profile for powder XRD data of $CaSrFe_{0.75}Co_{0.75}Mn_{0.5}O_{6-\delta}$ refined in the space group $Pm\bar{3}m$. Crosses represent experimental data, the solid red line is the model, vertical pink tick marks show Bragg peak positions, and the lower blue line represents the difference plot.

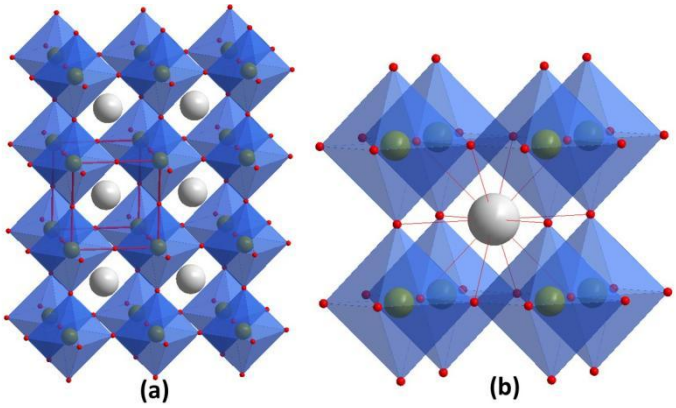

Figure 2. Crystal structure. (**a**) Crystallographic unit cell and corner-sharing $(Fe/Co/Mn)O_6$ octahedra (blue) are highlighted. The large whitish gray spheres are the Ca and Sr atoms; (**b**) Coordination geometry around the Ca/Sr atom, which is 12-coordinated, in a cubic unit cell.

Table 1. The unit cell parameters and Powder X-ray data refinement profile for $CaSrFe_{0.75}Co_{0.75}Mn_{0.5}O_{6-\delta}$.

Space Group	**Cell volume (Å^3)**	**a (Å)**	**Angles**	**wRp**	**Rp**	**χ2**
Pm-3m	56.092(4)	3.82796(5)	90^0	0.0423	0.0322	1.451
Elements	**x**	**y**	**z**	**multiplicity**	**occupancy**	**uiso**
Ca	0.5	0.5	0.5	1	0.5	0.0258(2)
Sr	0.5	0.5	0.5	1	0.5	0.0258(2)
Fe	0.0	0.0	0.0	1	0.375	0.0448(8)
Mn	0.0	0.0	0.0	1	0.250	0.0448(8)
Co	0.0	0.0	0.0	1	0.375	0.0448(8)
O	0.5	0.0	0.0	3	0.907	0.0587(6)

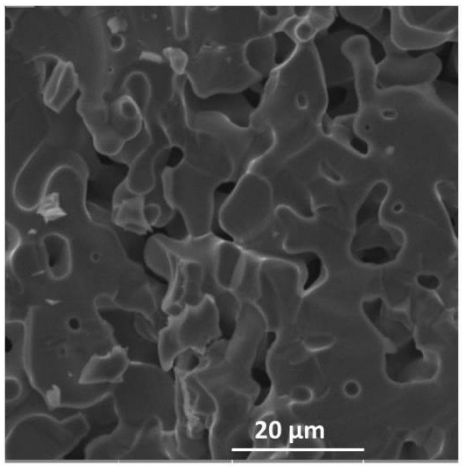

Figure 3. SEM image of $CaSrFe_{0.75}Co_{0.75}Mn_{0.5}O_{6-\delta}$.

3.2. Thermal Conductivity

Perovskite oxides exhibit a polycrystalline nature, wherein heat transfer occurs through a range of phonons with varying wavelengths and mean free paths [19,20]. The interference among thermal phonons hinders heat propagation [19]. Local lattice distortions, vacancies, and other factors act as sites for phonon scattering, leading to diminished thermal conductivity. Several elements contribute to the reduction in thermal conductivity of perovskite oxides, including crystal structure variations, grain size [21], grain boundaries [22,23], and oxygen vacancies. These factors increase phonon scattering, consequently decreasing lattice thermal conductivity.

The thermal conductivity reduction in our materials is not attributed to lattice distortion and structural transformation because the structure of $CaSrFe_{0.75}Co_{0.75}Mn_{0.5}O_{6-\delta}$ is usual cubic perovskite. In the pursuit of enhancing the performance of inorganic thermoelectric materials, researchers commonly reduce thermal conductivity by increasing phonon scattering to minimize lattice contribution. This can be achieved by introducing grain boundaries, where a greater number and more random distribution result in higher phonon scattering and lower thermal conductivity [22,24,25] but it is also not the case in our material as no clear grain boundaries are observed in the SEM image. Additionally, variations in grain size can affect phonon scattering, with smaller grain sizes contributing to increased phonon scattering and decreased thermal conductivity [21,25]. However, this is also not the case in our material because the grains look diffused without clear grain size.

Some reports focused on oxygen vacancy generation and its effectiveness in reducing thermal conductivity [23,26], while some highlighted the reduction in the mean free path of phonons as a responsible factor for thermal conductivity decrease [19,20]. Numerous studies on polycrystalline materials, such as perovskite oxides, emphasize the impact of oxygen (O) vacancies on phonon scattering and subsequent thermal conductivity reduction [23]. For instance, research on $(Ca_{0.25}Sr_{0.25}Ba_{0.25}Re_{0.25})TiO_3$ ceramics demonstrated a decline in thermal conductivity with an increase in oxygen vacancies, attributing this effect to point defect scattering and lowered symmetry [23]. O-vacancies can result in the reduction of the thermal conductivity of the lattice due to anisotropic phonon scattering at the vacancies [27].

Table 2 shows the thermal conductivities of the material at different temperatures ranging from 21 °C to 40 °C. The table shows that the thermal conductivity of $CaSrFe_{0.75}Co_{0.75}Mn_{0.5}O_{6-\delta}$ increases with the rise of temperature in the studied temperatures. The material under consideration exhibits a noteworthy thermal conductivity of 0.724 W/m/K at room temperature, indicating a high thermal insulation property. This characteristic can be discussed in terms of various factors influencing thermal conductivity. While the movement of electrons, particularly involving M^{3+} and M^{4+} spins (M = Fe, Co, Mn), may contribute to thermal conductivity, it is crucial to recognize that this phenomenon is multifaceted. In the realm of electron-doped materials, such as $CaMnO_3$ or $Ca_{0.9}R_{0.1}MnO_3$ (*R* = La, Pr, Nd, Sm, Eu, Gd, Tb, Dy, Ho, Er, Yb) the impact of phonon scattering becomes more prominent, overshadowing the roles of electrons and spins [28]. Similarly, studies on an oxygen-deficient compound related to $SrTiO_3$ highlight that phonon scattering has a dominant effect over electronic contributions [29]. The total thermal conductivity (K) is the sum of contributions from phonons (K_p) and photons (radiation)

K_R, as expressed by Equation (1) [30]. The components of K_p encompass contributions from grain boundaries, lattice, and point defects [30].

$$K = K_p + K_R \quad (1)$$

Increased phonon scattering typically leads to a reduction in thermal conductivity. Heat flow, involving phonons with different wavelengths and mean-free paths, encounters interference hindering efficient heat propagation. Factors such as local lattice distortions, structures with void spaces, and random vacancies act as sites for phonon scattering, resulting in decreased thermal conductivity.

Based on the consideration of all the possible influencing factors for the observed low thermal conductivity in our material, the suppression of lattice thermal conductivity and heightened phonon scattering can be primarily due to the presence of oxygen vacancies. This aligns with previous findings demonstrating how the introduction of oxygen vacancies can effectively suppress thermal conductivity. The porosity might have also contributed to the reduction of the thermal conductivity. In summary, oxygen vacancies play a pivotal role in enhancing phonon scattering and consequently reducing thermal conductivity in the studied compound.

Table 2. Thermal conductivities of $CaSrFe_{0.75}Co_{0.75}Mn_{0.5}O_{6-\delta}$ at different temperatures.

Temperatures (°C)	Thermal Conductivity (W/m/K)
21	0.701
25	0.724
30	0.793
35	0.856
40	0.951

4. Conclusions

The thermal conductivity of materials plays a pivotal role in determining their suitability for various applications, particularly in fields such as energy conversion and electronic devices. In this context, the oxygen-deficient perovskite $CaSrFe_{0.75}Co_{0.75}Mn_{0.5}O_{6-\delta}$ has emerged as a noteworthy subject of study due to its reported thermal conductivity of 0.724 W/m/K at 25 °C. This value not only underscores the efficient thermal insulation property of the material but also accentuates its potential significance in applications where effective heat management is essential. Exploring and understanding the thermal properties of $CaSrFe_{0.75}Co_{0.75}Mn_{0.5}O_{6-\delta}$ contributes not only to the advancement of material science but also opens avenues for the development of innovative technologies that rely on superior thermal insulation characteristics.

Funding

Instructional Capacity Excellence in TCUP Institutions (ICE-TI) award # 2225648 and NSF Tribal Enterprise Advancement Center award grant no. HRD 1839895.

Institutional Review Board Statement

Not Applicable.

Informed Consent Statement

Not applicable.

Acknowledgments

This work is supported in part by the National Science Foundation Tribal College and University Program Instructional Capacity Excellence in TCUP Institutions (ICE-TI) award # 2225648. A part of this work is also supported by NSF grant no. HRD 1839895. Additional support for the work came from ND EPSCOR STEM grants for the purchase of potentiostat and X-ray diffractometer. Permission was granted by United Tribes Technical Colleges (UTTC) Environ-mental Science Department to publish this information. The views expressed are those of the authors and do not necessarily represent those of United Tribes Technical College.

Conflicts of Interest

The authors declare no conflict of interest.

References

1. Cohen, R.E. Origin of ferroelectricity in perovskite oxides. *Nature* **1992**, *358*, 136–138. [CrossRef]
2. Tyunina, M. Oxygen vacancies in perovskite oxide piezoelectrics. *Materials* **2020**, *13*, 5596. [CrossRef]
3. Kim, M.; McNally, G.M.; Kim, H.H.; Oudah, M.; Gibbs, A.S.; Manuel, P.; Green, R.J.; Sutarto, R.; Takayama, T.; Yaresko, A. et al. Superconductivity in (Ba, K) SbO_3. *Nat. Mater.* **2022**, *21*, 627–633. [CrossRef]
4. Hona, R.K.; Ramezanipour, F. Remarkable oxygen-evolution activity of a perovskite oxide from the $Ca_{2-x}Sr_xFe_2O_{6-\delta}$ series. *Angew. Chem. Int. Ed.* **2019**, *58*, 2060–2063. [CrossRef]
5. Hona, R.K.; Karki, S.B.; Ramezanipour, F. Oxide electrocatalysts based on earth-abundant metals for both hydrogen-and oxygen-evolution reactions. *ACS Sustainable Chem. Eng.* **2020**, *8*(31), 11549–11557. [CrossRef]
6. Xu, X.; Wang, W.; Zhou, W.; Shao, Z. Recent advances in novel nanostructuring methods of perovskite electrocatalysts for energy-related applications. *Small Methods* **2018**, *2*, 1800071. [CrossRef]
7. Shu, L.; Sunarso, J.; Hashim, S.S.; Mao, J.; Zhou, W.; Liang, F. Advanced perovskite anodes for solid oxide fuel cells: A review. *Int. J. Hydrog. Energy.* **2019**, *44*, 31275–31304. [CrossRef]
8. Takeguchi, T.; Yamanaka, T.; Takahashi, H.; Watanabe, H.; Kuroki, T.; Nakanishi, H.; Orikasa, Y.; Uchimoto, Y.; Takano, H.; Ohguri, N.; et al. Layered perovskite oxide: A reversible air electrode for oxygen evolution/reduction in rechargeable metal-air batteries. *J. Am. Chem. Soc.* **2013**, *135*, 11125–11130. [CrossRef]
9. Hona, R.K.; Thapa, A.K.; Ramezanipour, F. An anode material for lithium-ion batteries based on oxygen-deficient perovskite $Sr_2Fe_2O_{6-\delta}$. *ChemistrySelect.* **2020**, *5*, 5706–5711. [CrossRef]
10. Hona, R.K.; Karki, S.B.; Cao, T.; Mishra, R.; Sterbinsky, G.E.; Ramezanipour, F. Sustainable oxide electrocatalyst for hydrogen-and oxygen-evolution reactions. *ACS Catal.* **2021**, *11*, 14605–14614. [CrossRef]
11. Hona, R.K.; Karki, S.B.; Dhaliwal, G.S.; Guinn, M.; Ramezanipour, F. High thermal insulation properties of $A_2FeCoO_{6-\delta}$ (A = Ca, Sr). *J. Mater. Chem. C.* **2022**, *10*, 12569–12573. [CrossRef]
12. Karki, S.B.; Hona, R.K.; Ramezanipour, F. Effect of structure on sensor properties of oxygen-deficient perovskites, $A_2BB'O_5$ (A = Ca, Sr; B = Fe; B′ = Fe, Mn) for oxygen, carbon dioxide and carbon monoxide sensing. *J. Electron. Mater.* **2020**, *49*, 1557–1567. [CrossRef]
13. He, J.; Xu, X.; Li, M.; Zhou, S.; Zhou, W. Recent advances in perovskite oxides for non-enzymatic electrochemical sensors: A review. *Anal. Chim. Acta.* **2023**, *1251*, 341007. [CrossRef]
14. Sahare, S.; Kumar, M.; Ghoderao, P.; Aepuru, R.; Lee, S.L.; Yun, J.H. Oxide perovskites and their derivatives for photovoltaics applications. In *Advanced Ceramics for Energy and Environmental Applications*, 1st ed.; CRC Press: Boca Raton, US, 2021.
15. Xu, X.; Pan, Y.; Zhong, Y.; Ran, R.; Shao, Z. Ruddlesden–Popper perovskites in electrocatalysis. *Mater. Horiz.* **2020**, *7*, 2519–2565. [CrossRef]
16. Martinson, A.; Guinn, M.; Hona, R.K. The crystal structure study of $CaSrFe_{0.75}Co_{0.75}Mn_{0.5}O_{6-\delta}$ by neutron diffraction. *J. Mater. Sci. Chem. Eng.* **2024**, *12*, 29–35. [CrossRef]
17. Zhang, M.; Zou, P.; Jeerh, G.; Sun, B.; Walker, M.; Tao, S. Oxygen vacancy-rich $La_{0.5}Sr_{1.5}Ni_{0.9}Cu_{0.1}O_{4-\delta}$ as a high-performance bifunctional catalyst for symmetric ammonia electrolyzer. *Adv. Funct. Mater.* **2022**, *32*, 2204881. [CrossRef]
18. Wang, S.; Han, P.; Zhao, Y.; Sun, W.; Wang, R.; Jiang, X.; Wu, C.; Sun, C.; Wei, H. Oxygen-vacancy-mediated $LaFe_{1-x}Mn_xO_{3-\delta}$ perovskite nanocatalysts for degradation of organic pollutants through enhanced surface ozone adsorption and metal doping effects. *Nanoscale.* **2021**, *13*, 12874–12884. [CrossRef]
19. Maire, J.; Anufriev, R.; Yanagisawa, R.; Ramiere, A.; Volz, S.; Nomura, M. Heat conduction tuning by wave nature of phonons. *Sci. Adv.* **2017**, *3*, e1700027. [CrossRef]
20. Snyder, G.J.; Toberer, E.S. Complex thermoelectric materials. *Nature Mater.* **2008**, *7*, 105–114. [CrossRef]
21. Delorme, F.; Chen, C.; Schoenstein, F.; Jaber, N.; Jean, F.; Bah, M.; Simon, Q.; Chartier, T.; Laffez, P.; Monot-Laffez, I.; et al. Low intrinsic thermal conductivity of Spark Plasma Sintered dense $KNbO_3$ and $NaNbO_3$ perovskite ceramics. *Thermochim. Acta.* **2021**, *695*, 178807. [CrossRef]
22. Bocher, L.; Aguirre, M.H.; Logvinovich, D.; Shkabko, A.; Robert, R.; Trottmann, M.; Weidenkaff, A. $CaMn_{1-x}Nb_xO_3$ ($x \leq 0.08$) perovskite-type phases as promising new high-temperature n-type thermoelectric materials. *Inorg. Chem.* **2008**, *47*(18), 8077–8085. [CrossRef]
23. Zhang, P.; Gong, L.; Lou, Z.; Xu, J.; Cao, S.; Zhu, J.; Yan, H.; Gao, F. Reduced lattice thermal conductivity of perovskite-type high-entropy $(Ca_{0.25}Sr_{0.25}Ba_{0.25}RE_{0.25})$ TiO_3 ceramics by phonon engineering for thermoelectric applications. *J. Alloys Compd.* **2022**, *898*, 162858. [CrossRef]

24. Wu, T.; Gao, P. Development of perovskite-type materials for thermoelectric application. *Materials* **2018**, *11*, 999. [CrossRef]
25. Vijay, V.; Harish, S.; Archana, J.; Navaneethan, M. Synergistic effect of grain boundaries and phonon engineering in Sb substituted Bi_2Se_3 nanostructures for thermoelectric applications. *J. Colloid Interface Sci.* **2022**, *612*, 97–110. [CrossRef]
26. Lou, Z.; Zhang, P.; Zhu, J.; Gong, L.; Xu, J.; Chen, Q.; Reece, M.J.; Yan, H.X.; Gao, F. A novel high-entropy perovskite ceramics $Sr_{0.9}La_{0.1}(Zr_{0.25}Sn_{0.25}Ti_{0.25}Hf_{0.25})$ O_3 with low thermal conductivity and high Seebeck coefficient. *J. Eur. Ceram. Soc.* 2022, *42*, 3480–3488. [CrossRef]
27. Zheng, W.; Cao, W.; Wang, Z.; Deng, H.; Shi, J.; Xiong, R. Improvement of the thermoelectric properties of a MoO_3 monolayer through oxygen vacancies. *Beilstein J. Nanotechnol.* **2019**, *10*, 2031–2038. [CrossRef]
28. Wang, Y.; Sui, Y.; Wang, X.; Su, W.; Liu, X.; Fan, H.J. Thermal conductivity of electron-doped $CaMnO_3$ perovskites: Local lattice distortions and optical phonon thermal excitation. *Acta Mater.* **2010**, *58*, 6306–6316. [CrossRef]
29. Rahman, J.U.; Nam, W.H.; Van Du, N.; Rahman, G.; Rahman, A.U.; Shin, W.H.; Seo, W.S.; Kim, M.H.; Lee, S. Oxygen vacancy revived phonon-glass electron-crystal in $SrTiO_3$. *J. Eur. Ceram. Soc.* **2019**, *39,* 358–365. [CrossRef]
30. Schlichting, K.W.; Padture, N.P.; Klemens, P.G. Thermal conductivity of dense and porous yttria-stabilized zirconia. *J. Mater. Sci.* **2001**, *36*, 3003–3010. [CrossRef]